Mapping Glacial Lakes in the Upper Indus Basin (UIB) Using Synthetic Aperture Radar (SAR) Data

Imran Khan *, Jennifer M. Jacobs, Jeremy M. Johnston, Megan Vardaman

Posted Date: 4 September 2025

doi: 10.20944/preprints202509.0422.v1

Keywords: upper indus basin; glacial lake inventory; SAR; adaptive thresholding

 doi:10.20944/preprints202509.0422.v1

Article

Mapping Glacial Lakes in the Upper Indus Basin (UIB) Using Synthetic Aperture Radar (SAR) Data

Imran Khan [1,2,*], Jennifer M. Jacobs [1,2], Jeremy M. Johnston [1,2] and Megan Vardaman [1,2]

[1] Department of Civil and Environmental Engineering, University of New Hampshire, Durham, NH, USA
[2] Earth Systems Research Center, Institute for the Study of Earth, Oceans, and Space, University of New Hampshire, Durham, NH, USA
* Correspondence: imran.khan@unh.edu

Abstract

Glacial lakes in the Upper Indus Basin (UIB) are rapidly evolving due to accelerated glacier retreat driven by climate change. Here we present a comprehensive inventory of glacial lakes using Sentinel-1 SAR data with adaptive backscatter thresholding, enabling consistent detection under challenging conditions and improving delineation accuracy. In August 2023, we identified 6,019 glacial lakes at scales from 0.001 to 5.80 km^2, covering a cumulative area of 266 km^2 (~0.06% of the basin). Although more than 90% of the lakes are smaller than 0.1 km^2, large lakes (>0.1 km^2) account for over 57% of the total lake area. Most lakes are concentrated between 4,000 and 4,600 m, coinciding with the main glacierized zone. Regional patterns reveal that the Hindu Kush and Himalayas are dominated by glacier erosion lakes (GELs) and moraine-dammed lakes (MDLs), reflecting widespread glacier retreat, whereas the Karakoram is characterized by numerous supraglacial lakes (SGLs) associated with extensive debris-covered glaciers. Compared to previous optical-based inventories, our SAR-based approach captures more lakes and better represents small and transient features such as SGLs. These findings provide a more accurate baseline for assessing cryospheric change and glacial lake hazards in one of the world's most heavily glacierized basins.

Keywords: upper indus basin; glacial lake inventory; SAR; adaptive thresholding

1. Introduction

Climate change is dramatically transforming glaciated regions around the world, resulting in widespread glacier mass loss and retreat [1–3]. This retreat is driving the accelerated formation and expansion of glacial lakes [4–6]. Between 1990 and 2018, the number of global glacial lakes (>0.05 km^2) increased by 53%, reaching a total volume of 156.5 km^3, which is a sea level equivalent of 0.43 mm [5]. A recent global inventory identified 117,352 glacial lakes (≥0.01 km^2), with a cumulative area of approximately 25,000 km^2 [7]. As ongoing glacier retreat and lake expansion accelerate under anthropogenic climate change, glacial lake outburst flood (GLOF) activity is also expected to increase significantly over the 21st century [8].

The distribution of glacial lakes at regional scales (e.g., High Mountain Asia (HMA), the Alps, the Andes, Greenland, and Alaska) has been extensively studied using remote sensing datasets, specifically optical imagery [4,9–14]. Particularly for the HMA region, which includes the Hindu Kush, Himalayas, Karakoram, Tienshan Mountains, and Tibetan Plateau, several glacial lake inventories have been created [6,15–18]. The first comprehensive glacial lake inventory for HMA manually delineated 27,205 and 30,121 glacial lakes (>0.0054 km^2), covering a combined area of 1,806 and 2,080 km^2 in 1990 and 2018, respectively [6]. Other important findings for the HMA include a total lake area increase of approximately 7% between 2008 and 2017 [18], and an annual expansion rate of 1.38% between 2008 and 2016 [17]. A summary of existing regional and global glacial lake inventories covering the HMA region is provided in the supplementary material (Table S1).

 doi:10.20944/preprints202509.0422.v1

In addition to optical remote sensing approaches, several recent studies have explored the use of synthetic aperture radar (SAR) data for glacial lake mapping. SAR offers significant advantages over optical data, particularly its ability to acquire images regardless of cloud cover or illumination conditions [19]. A variety of methods have been applied to SAR imagery for glacial lake detection, including simple backscatter thresholding, random forest classifiers, and deep learning algorithms [20–24]. To further improve detection accuracy, some studies have combined SAR and optical imagery to leverage the strengths of both sensors [25–27].

Despite the abundance of published studies and datasets, several key research gaps persist. One major limitation concerns the temporal scope of the imagery used. To minimize cloud and snow cover, studies often rely on satellite imagery spanning extended seasonal windows, for example, June to November [6], July to November [18], August to December [28], and even multiple years [15]. Such wide timeframes, which are even broader in global inventories, reduce the temporal specificity of lake conditions, making it difficult to capture glacial lake dynamics during a consistent seasonal period.

A second limitation involves the underrepresentation of highly dynamic supraglacial lakes (SGLs), which are typically short-lived and fluctuate at sub-seasonal to seasonal timescales [22,23,29]. These lakes are particularly susceptible to omission due to both their small size and transient nature. The use of extended windows for image selection contributes to their exclusion, as SGLs may appear and disappear between acquisition dates. Additionally, the application of minimum lake area thresholds introduces further bias against smaller water bodies. Consequently, regional-scale inventories that use coarser thresholds and wider acquisition windows systematically underrepresent small and short-lived lakes (Table S1).

While SAR-based techniques address several limitations inherent to optical data, significant challenges remain. Processing SAR data in glaciated mountainous terrain is complicated by the complex nature of radar backscatter [19,30,31]. Moreover, achieving broader spatiotemporal transferability of SAR-based mapping methods remains difficult and often requires extensive training datasets [21,22]. As a result, no regional-scale SAR-based glacial lake inventory currently exists for the HMA region.

This study addresses the limitations of existing glacial lake inventories by utilizing Sentinel-1 SAR imagery to develop a comprehensive inventory for the Upper Indus Basin (UIB), one of the most glacierized regions in the world and a critical water supply for Pakistan. Leveraging the all-weather data acquisition capabilities of SAR [26], the analysis is confined to a narrow observation window in August 2023, to reduce interference from seasonal snow. This narrow window also enhances the temporal consistency of lake detection. We also analyze the spatial distribution and characteristics of the mapped lakes and systematically compare them to existing inventories to assess discrepancies and highlight improvements.

2. Materials and Methods

2.1. Site Description

The UIB (Figure 1) is a transboundary river basin located in the high mountain ranges of the Hindu Kush, Karakoram, Himalayas, and the Tibetan Plateau, spanning parts of Afghanistan, Pakistan, India, and China, with a total area of approximately 425,000 km² [32]. With over 17,000 individual glaciers and a total glacierized area exceeding 25,000 km², the UIB is among the most glaciated areas on the planet [33–35]. Glacier melt contributes up to 40% of annual streamflow, with peak discharge occurring during the summer months when melt rates are highest [36,37]. River flows exhibit pronounced seasonality, primarily driven by snow and glacier melt [38]. This seasonal meltwater supply is critical for downstream communities and much of Pakistan, where it supports agriculture, hydropower generation, and industrial activities [32,38,39].

 doi:10.20944/preprints202509.0422.v1

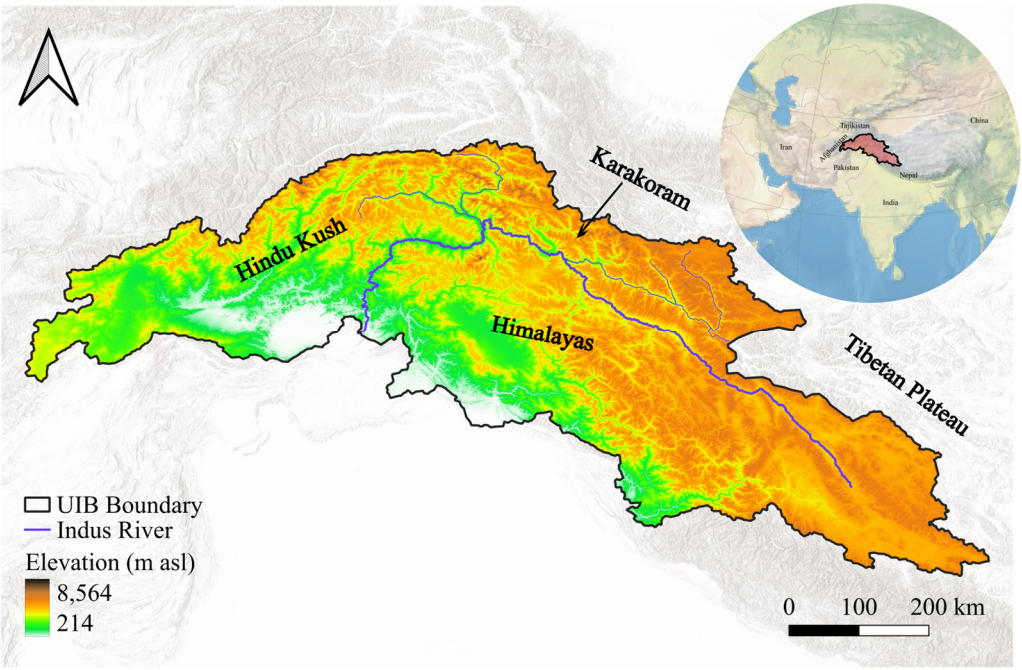

Figure 1. The Upper Indus Basin and its sub-regions. The elevation distribution is from the SRTM digital elevation models (DEMs).

The UIB has a complex climatology due to the interaction of multiple atmospheric circulation systems, including the westerlies and the Indian summer monsoon, and its highly variable topography [32,40,41]. According to the Köppen-Geiger classification, the region falls under a cold desert climate, characterized by warm, dry summers and cold winters [42]. The westerly flows, dominant during winters, are responsible for most of the total annual precipitation, while the Indian summer monsoon dominates during the summer months [43,44].

There is high variability in elevation across the UIB, ranging from 569 m in the valleys to over 8,000 m at mountain peaks, with a mean elevation of 3,750 m [45]. This topographic variation significantly influences spatial patterns of precipitation. Annual precipitation ranges from 100 to 200 mm in lower valleys, increases to approximately 600 mm around 4,400 m, and can exceed 1,500 to 2,000 mm above 5,500 m [43,46].

2.2. Data

For this study, we utilized multiple satellite and geospatial datasets to map glacial lakes. Our primary dataset was Sentinel-1A C-band SAR imagery (5.405 GHz, 5.6 cm), specifically the Ground Range Detected (GRD) collection available in Google Earth Engine (GEE). Sentinel-1A has a repeat cycle of 12 days, and the GRD product provides calibrated and geometrically corrected backscatter data at spatial resolutions of 10, 25, or 40 m and across various polarizations and modes [47,48]. We used the 10 m vertical transmit/vertical receive (VV) polarization and the Interferometric Wide Swath (IW) instrument mode data to delineate glacial lakes. VV polarization reduces interference from surface reflections and enhances the contrast between water and surrounding terrain, making it well-suited for glacial lake mapping [49].

To create normalized difference water index (NDWI), normalized difference snow index (NDSI) maps, and manually delineated validation datasets, we used Sentinel-2 MSI imagery with cloud cover below 10%. Slope masking was performed using digital elevation data from the Shuttle Radar Topography Mission (SRTM) [50]. The Randolph Glacier Inventory (RGI) glacier outlines were utilized to define the glacierized area [34].

2.3. Glacial Lake Mapping

 doi:10.20944/preprints202509.0422.v1

The glacial lake mapping process involved three primary steps: (1) data preprocessing and preparation, (2) water body detection and lake delineation, and (3) accuracy assessment. Each step is described in the following subsections.

2.3.1. Data Preparation

Sentinel-1 GRD imagery in IW mode with VV polarization for August 2023 was filtered by date and study area and imported into GEE. While the GRD collection is already preprocessed to generate a calibrated and ortho-corrected product through thermal noise removal, radiometric calibration, and geometric correction [51], additional preprocessing was required to correct radiometric distortions and mitigate speckle noise. SAR datasets suffer from terrain-induced distortions and speckle noise due to radar backscatter interference [47,51,52]. The terrain flattening involved computing the local incidence angle by combining the radar incidence angle from the SAR image with terrain slope and aspect from the SRTM DEM, followed by gamma-nought normalization [53] using Equation 1,

$$\gamma^{\circ} = \frac{\sigma^{\circ}}{\cos(\theta_{LIA})} \qquad \text{Equation 1}$$

where γ° is the normalized backscatter, σ° represents the backscatter on a linear scale, and θ_{LIA} is the local incidence angle. The normalized backscatter was converted back to the dB scale and renamed as the new VV band.

To reduce noise while preserving features, we applied a 3x3 median filter, which replaces the center pixel intensity with the median of its eight neighboring pixels. This approach effectively suppresses extreme outliers while maintaining spatial details [23]. Where available, Sentinel-1 images from ascending and descending orbits with similar acquisition dates were combined to generate a median image. This step further reduced speckle noise and mitigated shadow effects, enhancing the quality of the data for glacial lake detection [27,54].

In addition to SAR data, auxiliary datasets were prepared to mask irrelevant features. An NDSI mask was generated from cloud-free Sentinel-2 MSI imagery, when available, to filter snow-covered areas. A slope mask was used to remove regions with slopes greater than 20 degrees, which commonly introduce classification errors due to terrain-induced radar scattering. These preprocessing steps significantly improved computational efficiency and reduced misclassifications caused by wet snow and mountain shadows, which exhibit backscatter values similar to glacial lakes.

2.3.2. Glacial Lake Delineation

The final preprocessed SAR dataset was used for lake delineation. Potential water bodies were initially identified using a lenient SAR backscatter threshold of -13 dB, classifying pixels with backscatter values below this threshold as water. Previous studies have employed a -14 dB threshold for glacial lake delineation in the Himalayas [26]. However, to minimize the exclusion of smaller lakes, a less restrictive threshold of -13 dB was used in this study. This simple thresholding approach led to the inclusion of some non-lake features, such as glacial ice, seasonal snow, and rugged terrain, resulting in classification errors. The water mask was vectorized into individual polygons, and key geometric and topographic attributes were extracted, including surface area, perimeter, and shape index (perimeter-to-area ratio). We applied a minimum shape index filter (0.2) to eliminate highly irregular-shaped non-lake features.

Since a global backscatter threshold is ineffective for accurately delineating glacial lakes of varying sizes, compositions, and surrounding features, we applied an adaptive thresholding method based on the Otus algorithm to reclassify the filtered polygons [55]. The Otsu algorithm analyzes the image histogram to obtain the variance for every possible threshold value and calculates the threshold that minimizes the inter-class variance. First, a buffer equal to the area was applied to each lake. For each buffered lake polygon, the Otsu algorithm was applied to identify the optimal backscatter threshold. We then used the optimized backscatter thresholds for each buffered polygon to reclassify them and obtain the final lake polygons. The associated attributes, including surface area, mean elevation, and centroid coordinates, were recalculated, and the lakes were filtered by a

 doi:10.20944/preprints202509.0422.v1

minimum lake area threshold of 1,000 m². This threshold was chosen to balance mapping accuracy with the retention of essential lake information. The lake polygons were overlaid onto false-color Sentinel-2 MSI composites for quality control. Manual inspection was conducted to remove false positives. Additionally, a few overestimated lake boundaries caused by surrounding ice were corrected manually using an NDWI mask. The final lake polygons, along with associated attributes including surface area, mean elevation, and centroid coordinates, were exported as shapefiles for further analysis.

The lakes were categorized into three major groups:

1. Supraglacial lakes (SGLs) form in topographical depressions on the surface of glaciers;
2. Moraine-dammed lakes (MDLs) form behind terminal or lateral moraines;
3. Glacial erosion lakes (GELs) form in topographical depressions in the bedrock.

SGLs were identified using glacier outlines from the RGI inventory, while MDLs and GELs were identified by analyzing their location and distance from current glaciers, comparing with previous inventories, and through visual inspection using a false color composite of Sentinel-2 optical imagery.

2.3.3. Accuracy Assessment

To evaluate the accuracy of the SAR-based glacial lake mapping, we manually delineated 65 lakes using Sentinel-2 MSI false-color composites. This validation dataset included glacial lakes of various sizes and types across the UIB. This dataset served as the reference for validating the lake mapping approach. We assessed the accuracy using mean absolute error (MAE), mean absolute percentage error (MAPE), root mean square error (RMSE), and the coefficient of determination (R^2). These metrics quantify both the magnitude of error and the agreement between SAR-derived and reference lake areas. The MAE and MAPE were obtained using Equations 2 and 3, respectively, as follows

$$MAE = \frac{1}{n}\sum_{i=1}^{n}|Area_{S2} - Area_{S1}| \quad \text{Equation 2}$$

$$MAPE = \frac{100}{n}\sum_{i=1}^{n}\left|\frac{Area_{S2} - Area_{S1}}{Area_{S2}}\right| \quad \text{Equation 3}$$

where n is the number of lakes in the validation dataset, $Area_{S1}$ is the area of each lake obtained from the Sentinel-1 imagery, and $Area_{S2}$ is the area obtained using manual delineation from Sentinel-2 optical imagery.

2.3.4. Glacial Lake Size Distribution

We assessed the statistical distribution of glacial lake sizes in the UIB using the powerlaw Python package, which evaluates the plausibility of power-law models relative to alternative distributions [56]. A power-law model was fitted to the observed lake size data, and the power-law exponent (α) and was estimated for lakes exceeding a minimum area threshold (x_{min}). This follows the general form of the power-law model:

$$P(x) \propto x^{-\alpha}, \quad \text{for } x \geq x_{min}$$

where P(x) is the probability of observing a glacial lake of area x.

The Python package automatically determined the minimum lake area threshold through an iterative procedure that identifies the cutoff yielding the best fit, based on minimizing the Kolmogorov-Smirnov (KS) statistic and maximizing the p-value (Clauset et al. 2009). The KS statistic represents the maximum difference between the empirical and fitted cumulative distribution functions. This analysis was applied across the entire UIB and repeated for each of its four major subregions and lake types to assess variations in scaling behavior.

3. Results

3.1. SAR-Based Lake Mapping and Accuracy Assessment

The automated SAR-based lake outlines demonstrate a high level of agreement with the manually digitized lakes from Sentinel-2 optical imagery, as illustrated by the 1:1 plot (Figure 2) and

 doi:10.20944/preprints202509.0422.v1

the overlapping lake outlines (Figure 3). The MAE and MAPE are 0.013 km² and 8.18%, respectively, with minimal bias (0.002 km²) (full Willmott statistics in Table S2). The SAR-based estimated lake areas (mean = 0.274 km²) are equivalent to manually delineated lake areas (mean = 0.272 km²) on average. For a few moraine-dammed lakes in contact with glacier ice, areas are overestimated by the SAR-based method, likely due to the low backscatter contrast between water and adjacent ice or wet snow, leading to boundary misclassifications, as illustrated in Figures 3e and 3f.

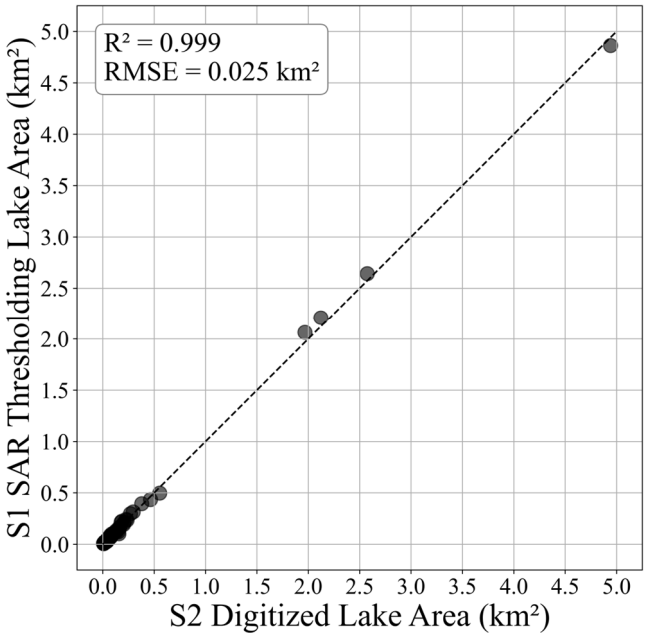

Figure 2. 1:1 comparison of glacial lake areas derived from Sentinel-1 (S1) SAR and manually digitized Sentinel-2 (S2) imagery. The strong agreement highlights the accuracy of the SAR-based approach.

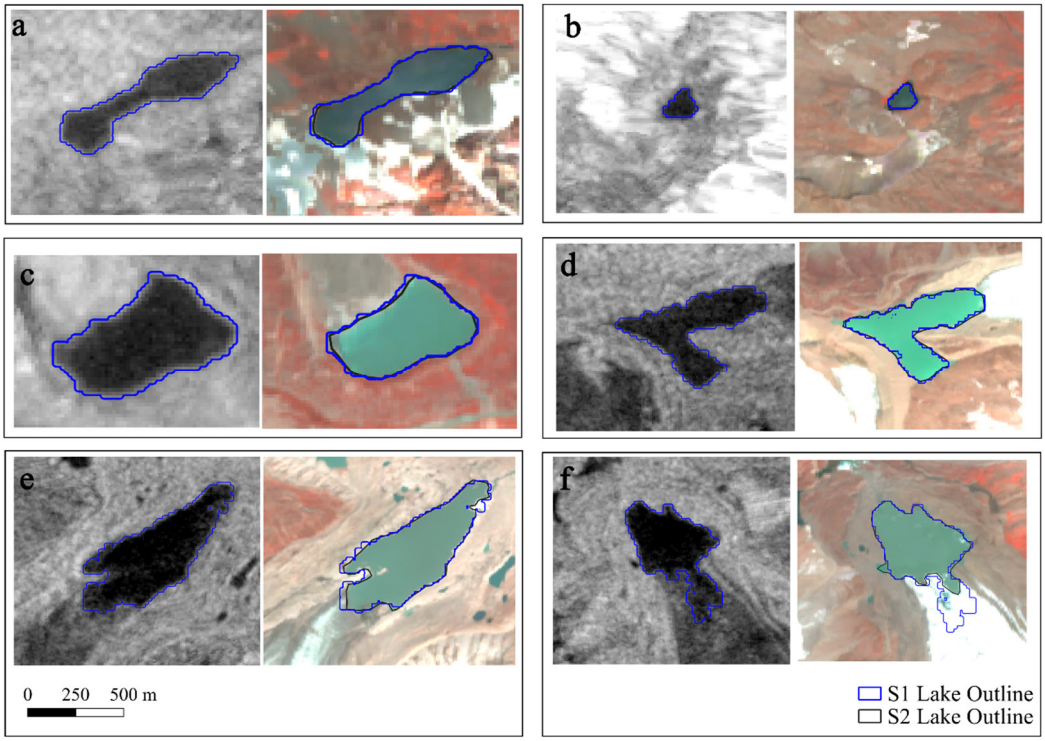

 doi:10.20944/preprints202509.0422.v1

Figure 3. Comparison of glacial lake outlines derived from Sentinel-1 SAR (blue) and Sentinel-2 optical imagery (black) for six lakes. Outlines are overlaid on Sentinel-1 SAR (left) and Sentinel-2 optical imagery (right). The visual comparison highlights close agreement for most lakes, with slight overestimation observed for ice-contact lakes using the SAR-based method (e and f).

Otsu-derived backscatter thresholds range from –13 to –28 dB, with a mean of –20 dB. The variability in threshold values, and their relationship with lake characteristics such as area and shape, underscores the importance of adaptive thresholding (Figure 4). A strong negative relationship was observed between lake area and threshold values (Spearman's $\varrho = -0.74$, $p < 0.001$), indicating that larger lakes tend to require lower thresholds. This reflects the fact that expansive water surfaces are easier to classify due to their more homogeneous backscatter. In contrast, lake shape shows a significant positive relationship with threshold values ($\varrho = 0.77$, $p < 0.001$). Lakes with higher shape indices, reflecting more irregular outlines, require higher thresholds to achieve accurate delineation.

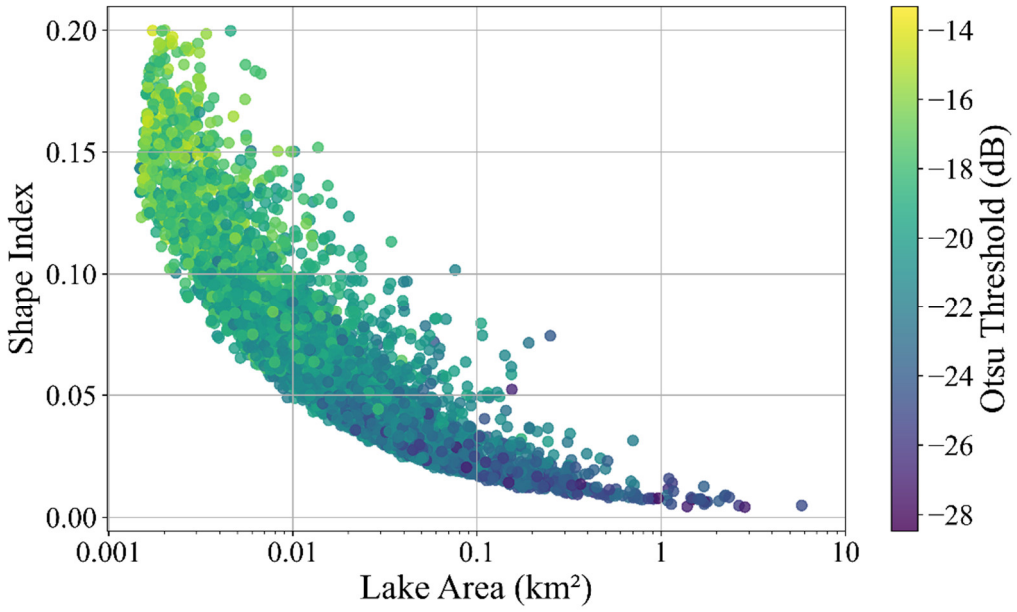

Figure 4. Scatter plot of lake area (log scale) versus shape index, with the color gradient representing the Otsu threshold.

3.2. Glacial Lake Area and Elevation Distribution

A total of 6,019 glacial lakes larger than 0.001 km² were identified across the UIB (Figure 5a), covering a cumulative area of 266 km², equivalent to 0.06% of the basin area (Table 1). Lake sizes range from 0.001 to 5.80 km², with a mean area of 0.04 km². Of these, 39.16% of the lakes are classified as small (< 0.01 km²), 53.08% as medium (0.01 to 0.1 km²), and 7.76% as large (> 0.1 km²). Despite their low frequency, large lakes account for 57% of the total lake area, while small lakes contribute only 4%.

The lake elevations range from 2,557 to 6,005 m, with peak lake concentrations between 4,000 and 4,600 m (Figure 5b). The median lake area remains relatively consistent across higher elevation bands. At the lowest elevations (2,400 – 2,600 m), the largest median areas (approximately 0.16 km²) occur, driven primarily by a few large lakes in the Himalayas and the Hindu Kush. Between 2,800 and 3,000 m, the median area declines sharply to its minimum (0.002 – 0.004 km²), reflecting the dominance of numerous small SGLs in the Karakoram. Above 3,400 m, the median area remains relatively small but stable at around 0.015 km² up to 5,800 m.

 doi:10.20944/preprints202509.0422.v1

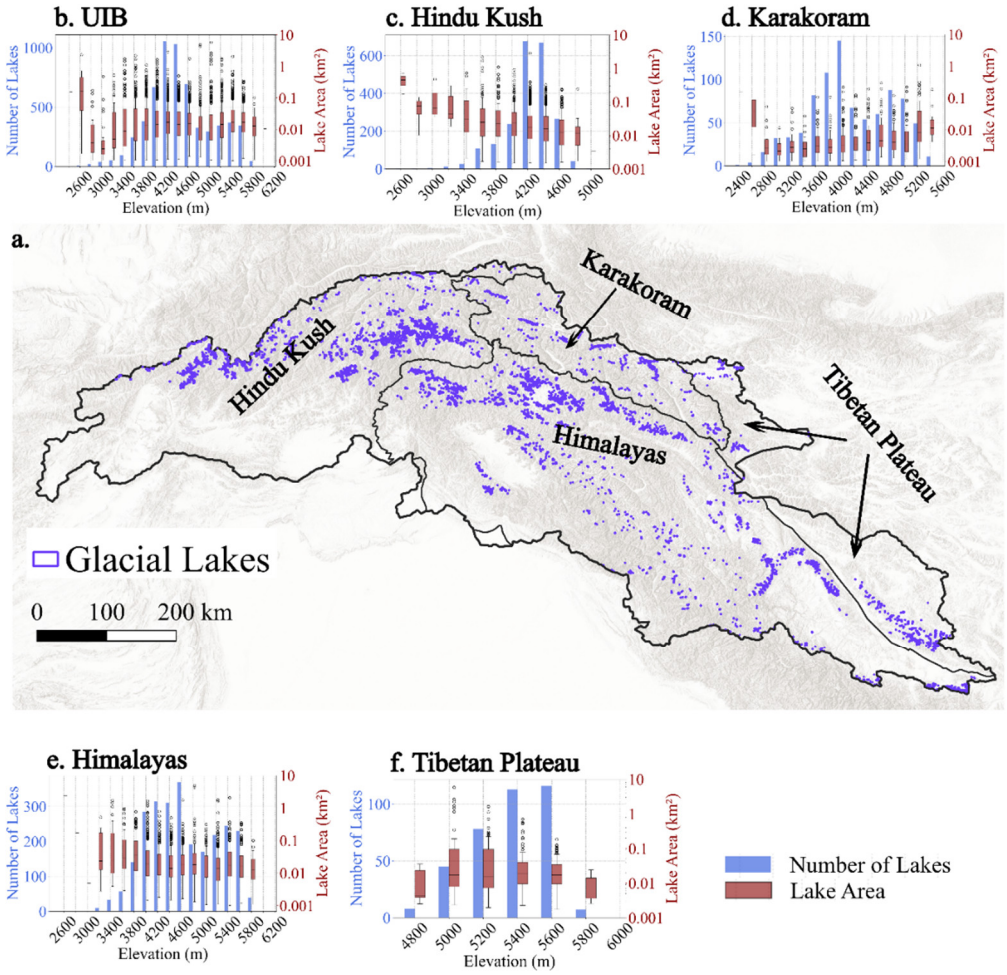

Figure 5. Glacial lake distribution and characteristics across the study area and sub-regions. (a) Map of the UIB study area, showing sub-region boundaries and delineated lakes (blue). (b) Number of lakes and lake area by elevation for the entire UIB basin, with lake counts shown as bars and lake area as boxplots within 200 m elevation bins. (c-f) Similar elevation-based distributions for the sub-regions: Hindu Kush, Karakoram, Himalayas, and Tibetan Plateau, respectively.

Table 1. Lake statistics, including lake number, size distributions, and mean elevation in the UIB and its sub-regions.

Region	Basin Area (km²)	Lake Count	Total Lake Area (km²)	% of Basin Area	Mean Area (km²)	Mean Lake Elevation (m)
UIB	425,000	6,019	266.0	0.06	0.044	4,566
Hindu Kush	134,000	2,171	89.4	0.06	0.041	4,323
Karakoram	40,000	866	11.4	0.03	0.013	4,249
Himalayas	201,000	2,615	129.6	0.06	0.050	4,747
Tibetan Plateau	50,000	367	35.6	0.07	0.100	5,469

The Himalayas and Hindu Kush, which collectively occupy a significant portion of the UIB, have the highest number of lakes with 2,615 and 2,171, and cover total areas of 129.6 km² and 89.4 km²,

 doi:10.20944/preprints202509.0422.v1

respectively. In both regions, medium-sized lakes dominate by count, comprising 59% of the total, and contribute 38-47% to the cumulative area. Large lakes, although fewer in number (7-9%), account for a substantial share of the lake area (48-58%). Similar to the overall UIB, most lakes are concentrated between 4,000 to 4,600 m elevations in these two sub-regions, with a slight decrease in median area with elevation (Figures 5c and 5e).

The Karakoram has 866 lakes and a comparatively smaller total lake area of 11.4 km^2. The region is dominated by small lakes (81% by count). However, the few large lakes (3%) contribute 44% to the total lake area. Most lakes are found between 3,600 and 4,200 m, and the median lake area, which is the lowest among the sub-regions, shows slight increase with elevation (Figure 5d).

The Tibetan Plateau's 367 lakes cover 35.6 km^2, over three times the lake area of the 866 Karakoram lakes. Large lakes, accounting for 12% of the total number, contribute a substantial 79% of the total lake area, highlighting their dominance. Medium-sized lakes make up 58% of the count but contribute only 18% of the area. This region is characterized by higher elevations, and its lakes are distributed between 4,800 and 6,000 m (Figure 5f).

3.2. Glacial Lake Type Distribution

Glacial lake types across the UIB and its sub-basins show distinct regional patterns (Figure 6). At the basin scale, GELs and MDLs dominate, comprising 54% and 34% of all lakes, and contributing 61% and 37% to the total lake area, respectively. Although SGLs represent 12% of the lake count, they account for only 2% of the total area. In terms of typical size, GELs and MDLs have similar median areas (0.018 and 0.017 km^2, respectively), whereas SGLs are distinctly smaller with a median area of 0.003 km^2.

The Himalayas, Hindu Kush, and Tibetan Plateau show broadly similar distributions, all characterized by the dominance of GELs and MDLs, which together account for >96% of the total count and >98% of the cumulative area. SGLs are rare in the Himalayas and Hindu Kush, contributing less than 1% to the total lake area, and are entirely absent in the Tibetan Plateau.

The Karakoram sub-region has a markedly different distribution of glacial lake types. Here, SGLs are the most prevalent, comprising 77% of the lakes and 40% of the total lake area. Although MDLs represent only 20% of the lakes, they account for the largest share of the area (54%), reflecting their larger typical sizes relative to SGLs. GELs are rare in the Karakoram, contributing just 2% of the lake count and about 6% of the cumulative area.

 doi:10.20944/preprints202509.0422.v1

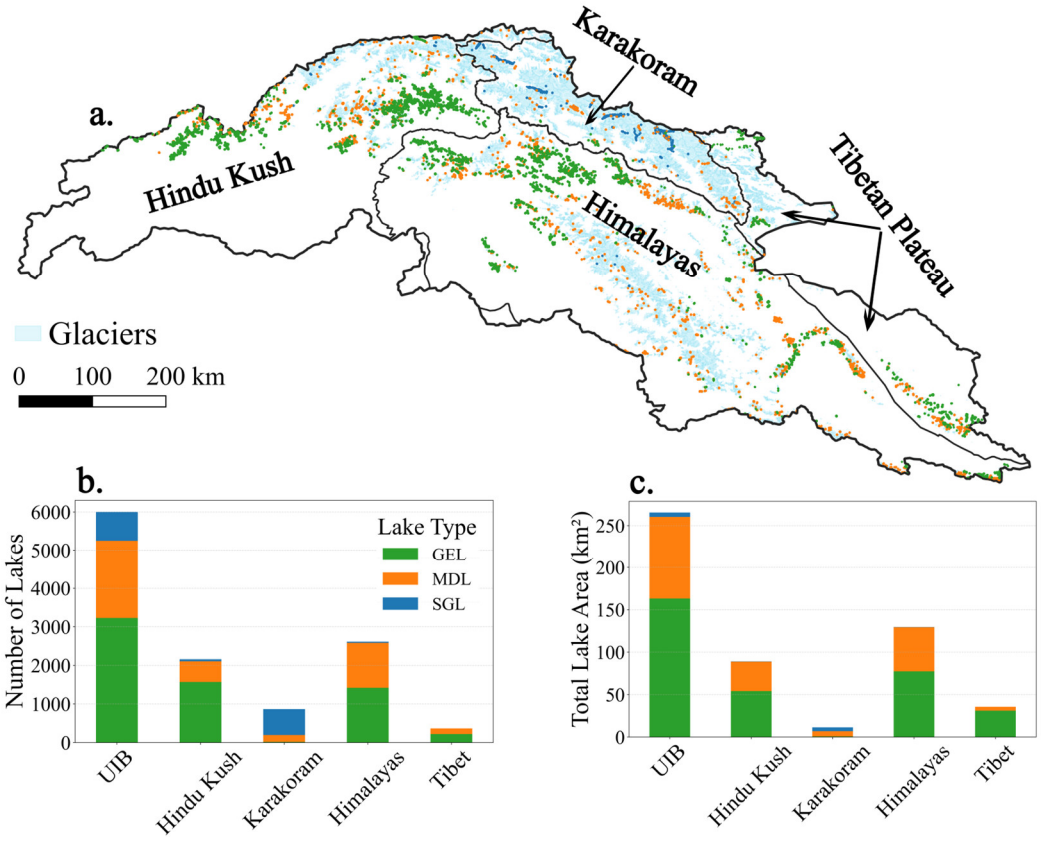

Figure 6. Distribution of glacial lake types across the UIB study area and sub-regions. (a) Map of the study area, showing the distribution of glaciers and glacial lakes in the UIB. Stacked bar plots showing (b) the number of lakes and (c the cumulative lake area by lake type (GEL, MDL, SGL) across the UIB and the four sub-regions (Hindu Kush, Karakoram, Himalayas, and Tibetan Plateau).

3.2. Power Law Distribution of Glacial Lake Area

The size distributions of glacial lakes in the UIB follow power-law behavior, indicating that small lakes are far more abundant than large ones (Figure 7). Across the entire basin, the power-law exponent (α) is 2.26 with a minimum lake area of 0.059 km^2.

The lake size distributions for the subregions have varying scaling behavior and minimum lake area thresholds (Table S3). The Himalayas exhibit a similar power-law distribution (α = 2.20) as the UIB, with a slightly lower area threshold of 0.041 km^2. In the Hindu Kush, the power-law fit was limited to the largest lakes (x_{min} = 0.118 km^2) with a steep slope (α = 2.67), reflecting the strong dominance of small lakes and scarcity of large ones.

In contrast, the Karakoram displays a much flatter slope (α = 1.91, x_{min} = 0.003 km^2), implying a higher relative frequency of large lakes. The scaling holds for very small lakes compared to other regions. The Tibetan Plateau has the flattest slope overall (α = 1.79, x_{min} = 0.016 km^2), consistent with the prevalence of large lakes.

Scaling also varies by lake type (Figure 7f, g, h). GELs follow a steep slope (α = 2.32, x_{min} = 0.07 km^2), reflecting the dominance of smaller lakes. MDLs show a slightly flatter slope (α = 2.19, x_{min} = 0.04 km^2), indicating a relatively greater contribution from larger lakes, although both types are overall dominated by small lakes. SGLs also show steep scaling (α = 2.30), but with a very low threshold (x_{min} = 0.005 km^2), reflecting their smaller sizes and high abundance.

The scaling analysis highlights two distinct regimes of glacial lake size distributions across UIB. The Himalayas and Hindu Kush exhibit steeper exponents, indicating that lake size distributions decay rapidly and that large lakes are relatively scarce. In contrast, the Karakoram and Tibetan Plateau have flatter slopes, reflecting a more gradual decay of the size distribution and a greater

 doi:10.20944/preprints202509.0422.v1

relative contribution from large lakes. In all cases, the lake size distributions deviate from power-law behavior below the estimated x_{min}, reflecting a relative scarcity of the smallest lakes compared to what would be expected under strict scaling.

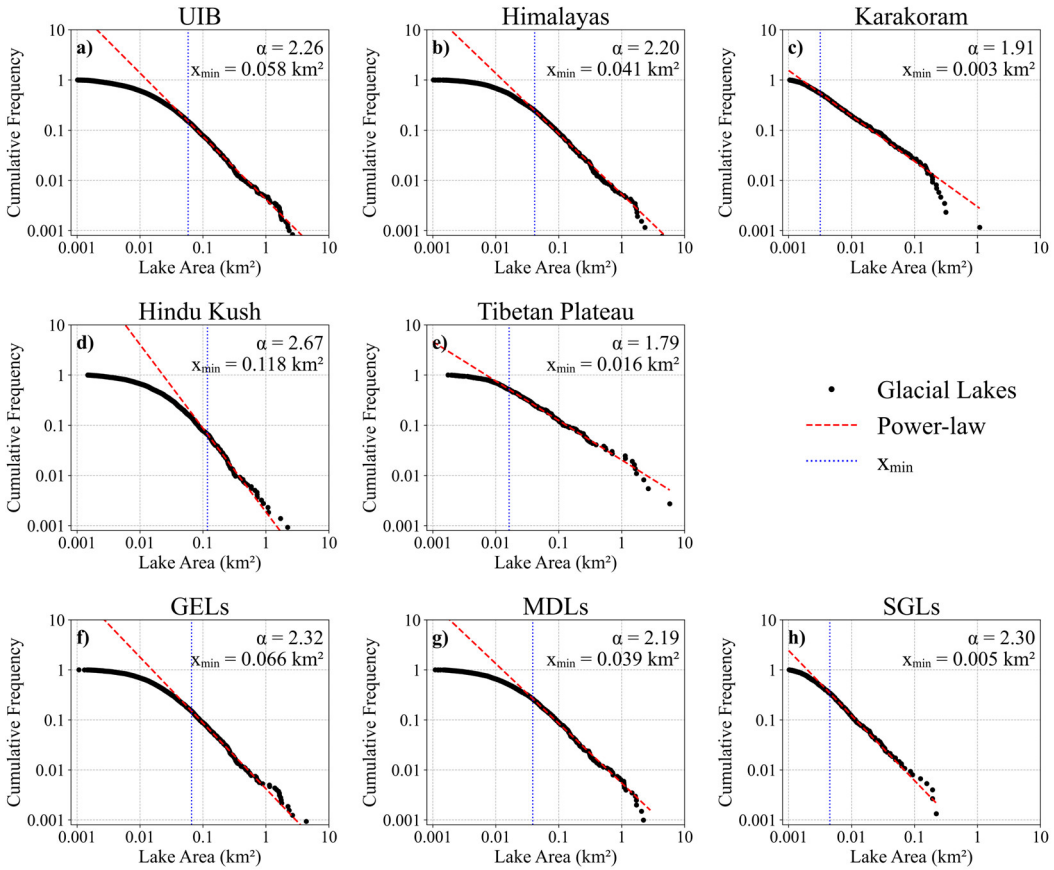

Figure 7. Complementary cumulative distribution functions (CCDF) of glacial lake areas in the UIB, its subregions, and lake types. Each subplot displays observed lake size distributions (black circles), fitted power-law models (red dashed lines) above a region-specific minimum threshold (blue dotted line). Power-law exponents (α) and minimum area threshold (xmin) are shown for each group.

4. Discussion

4.1. SAR-Based Glacial Lake Inventory and Comparison with Other Datasets

SAR offers a viable alternative to optical remote sensing-based glacial lake delineation, as it enables delineation under cloud cover and variable illumination conditions. In this study, we combined Sentinel-1 SAR data with adaptive backscatter thresholding to generate a new inventory of glacial lakes in the UIB. The SAR-based outlines show strong agreement with manually digitized reference lakes, confirming the reliability of the approach. Minor overestimation occurred where lakes bordered wet snow or glacier ice, likely due to the similarly low backscatter characteristics of these adjacent surfaces, a challenge also noted in previous SAR-based studies [20,57]. In addition, manual corrections were required to exclude misclassifications in such areas, highlighting a key limitation of SAR-based delineation where surface types have overlapping backscatter signatures.

To evaluate consistency with existing inventories, we compared our results with the dataset of Wang et al. (2020) [6]. After filtering their data to match our study area, Wang et al. (2020) [6] mapped 4,035 glacial lakes (≥ 0.0054 km²) covering a total area of 220.8 km² in 2018. In comparison, our 2023 SAR-based inventory identified 6,019 lakes (≥ 0.001 km²) in 2023, covering a total area of 266 km². When we applied the same minimum area threshold (≥ 0.0054 km²), our dataset contained 4,617 lakes covering 261.8 km², showing 87% agreement in lake number and 84% agreement in cumulative area

 doi:10.20944/preprints202509.0422.v1

relative to Wang et al. (2020) [6]. When both inventories were further aggregated to a 0.1° × 0.1° grid, 1:1 comparison plots for lake count and area showed very strong agreement between the two inventories (Figure 8).

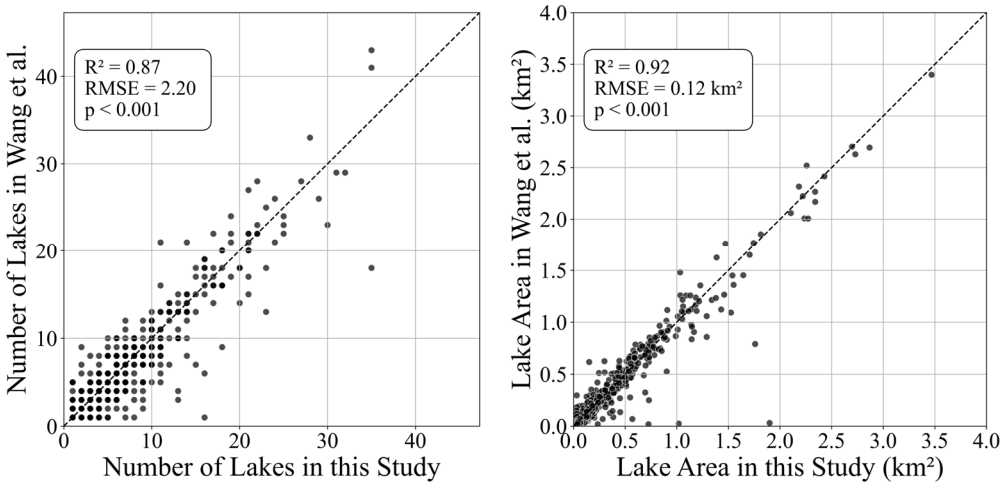

Figure 8. Comparison of (a) total lake area and (b) number of lakes per 0.1° × 0.1° grid cell between this study (filtered for lakes ≥ 0.0054 km²) and the dataset of Wang et al. (2020) [6] for 2018. Each point represents a grid cell where both datasets report lakes. The dashed line denotes the 1:1 line. While the lake area shows strong agreement between datasets, the lake count plot indicates that this study generally reports more lakes per cell, suggesting greater sensitivity to detecting smaller lakes.

The higher lake count and total area in our inventory compared to Wang et al. (2020) [6], even after applying the same minimum area threshold, can be attributed to several factors. First, our inventory is based on 2023 data, whereas Wang et al. (2020) [6] mapped lakes in 2018. Given the continued retreat of glaciers and the observed global trend of glacial lake expansion [3,5], some increase in lake number and area is expected over the five-year period. However, consistent and comparable mapping techniques are needed to identify trends over time in the number and size of lakes. Second, the use of Sentinel-1 SAR imagery in our study enabled consistent lake detection under cloudy or shadowed conditions, where optical sensors often face limitations [26]. However, while post-processing steps minimized major delineation errors, some overestimation of lake extents may persist in our results, potentially contributing to the slightly higher cumulative area compared to the optical-based inventory.

Finally, our analysis was restricted to a single month (August), to coincide with peak meltwater availability and increase the likelihood of capturing seasonally transient SGLs. In contrast, Wang et al. (2020) [6] used a broader observation window (June to November), which may have led to the omission of short-lived lakes. This difference, combined with the all-weather capabilities of SAR, likely contributed to the 223 SGLs identified in our inventory compared to 91 in Wang et al. (2020) [6]. This comparison highlights the strengths of SAR-based mapping, particularly in high-mountain regions with persistent cloud cover and dynamic lake evolution. Given its ability to penetrate cloud cover and capture dynamic lakes, such as the SGLs, our SAR-based approach likely offers a more comprehensive inventory of glacial lakes in the UIB. Additionally, the temporal update to 2023 provides a more current representation of lake distribution compared to earlier inventories.

3.2. Spatial Characteristics of Glacial Lake Distribution

The spatial distribution and characteristics of glacial lakes are influenced by glacier dynamics, topographic controls, and climatic influences [9,58]. The lake size, spatial, and altitudinal distribution in UIB are consistent with observations from other mountain regions. Across the UIB, lake size is

 doi:10.20944/preprints202509.0422.v1

skewed toward small and medium lakes by number, while a relatively small number of large lakes (> 0.1 km²) account for more than 50% of the total lake area. An abundance of smaller lakes is common across the glaciated regions. For example, in the Alps, lakes larger than 0.1 km² made up only 14% of the total lakes but accounted for 52% of the total lake area [11]. In the UIB, most glacial lakes are concentrated between 4,000 and 4,600 m in elevation, coinciding with the elevation range where the majority of glaciers are located [59,60]. Large lakes are typically found at lower elevations compared to small and medium lakes, a pattern attributed to the flatter terrain in these areas, which offers more favorable conditions for lake formation and expansion [11,61]. This relationship between terrain and lake development was particularly evident on the flatter Tibetan Plateau, where some of the largest lakes in the study area are located [62]. Additionally, increasing precipitation and warming temperatures since the late 1990s, along with permafrost degradation, have contributed to ongoing lake growth in this region [63,64].

GELs and MDLs are the most prevalent lake types in the UIB. Their dominance has been observed in other regions, including the greater Himalayas [58,65–68], the Tibetan Plateau [69], the Alps [12,70], the Andes [4,71], and Canada [72]. The abundance of GELs and MDLs is indicative of an advanced stage of glacier retreat, leading to the construction of substantial moraine dams and exposure of overdeepened bedrock basins, where MDLs and GELs form [9,14,73,74]. Most GELs are detached from active glaciers and respond more to changes in regional water balance than to direct glacier melt [14,75].

Across the subregions, glacial lake abundance is highest in the Himalayas and Hindu Kush, dominated by GELs and MDLs. This pattern reflects widespread glacier retreat, the presence of substantial moraines, and suitable topography for lake impoundment. In the Himalayas, approximately 40% of glacier area has been lost since the Little Ice Age (LIA), consistent with the widespread occurrence of GELs and MDLs [76]. Based on the RGI glacier outlines, currently both the Himalayas and Hindu Kush subregions have a 4% glacierized area [34]. In contrast, the Karakoram shows limited glacier area loss, with only 6.6% decline since the LIA, while some glaciers are advancing or showing stable mass balance [77,78]. Glacier cover remains extensive, at 41% of the total area. Under these conditions, the region is predominantly characterized by SGLs. The smaller number of MDLs and GELs in the Karakoram region, as opposed to their dominance in the Himalayas and Hindu Kush, shows the influence of the Karakoram Anomaly on glacial lake formation dynamics. With glacier stability and surge behavior dominating in this region, bedrock depressions and moraine dams are not available for extensive GEL and MDL formation, while the debris-covered flatter ablation zones of the Karakoram glaciers support extensive SGL formation.

The formation of SGLs is closely associated with debris-covered glacier tongues [18,79]. Extensive debris cover in this region leads to differential thinning of glaciers, enabling meltwater to accumulate in depressions on glacier surfaces [80,81]. SGL area is positively correlated with debris-covered glacier area and the glacier length, because longer glaciers provide ideal conditions for the coalescence of supraglacial ponds [18,79,82]. SGLs are typically smaller, more variable, and transient compared to GELs and MDLs [14,54]. However, they can coalesce and evolve into larger moraine-dammed lakes, influencing glacier dynamics and stability [83,84]. For example, lake-terminating glaciers experience enhanced surface lowering, retreat, and increased ice velocities, as observed in parts of the Himalayas [85–87]. The varying composition and dynamics of glacial lake types across the UIB thus provide valuable insights into regional glacier behavior and the broader impacts of climate change on high mountain hydrology.

3.2. Power-Law Distribution of Glacial Lake Area

The power-law behavior observed in the UIB and its subregions highlights the scale-invariant nature of glacial lake size distributions. However, variations in the power-law exponent and minimum area threshold across the subregions reflect the influence of regional geomorphology and dominant lake types. For example, the prevalence of smaller-sized SGLs on the debris-covered glaciers of Karakoram led to a power-law adherence that extended to lakes an order of magnitude

 doi:10.20944/preprints202509.0422.v1

smaller than other regions. In the Hindu Kush and Himalayas, where GELs and MDLs dominate, scaling applies only above larger minimum sizes compared to the SGL-rich Karakoram.

The power-law distribution of glacial lake sizes in the UIB is consistent with scaling behavior observed in other mountainous and glaciated regions for lake inventories [88,89] and in lake volume-area scaling [90,91], supporting the universality of such patterns in hydrological and geomorphological processes [92,93]. Most of the studies' minimum areas are an order of magnitude larger than this study. For example, Cael and Seekell (2016) [88] reported $\alpha = 2.14$ for global lakes ≥ 0.46 km^2; by comparison, our study yields $\alpha = 2.26$ for lakes ≥ 0.06 km^2. Levenson et al. (2025) [89] found $\alpha = 2.23$ for Alaskan glacial lakes ≥ 1.01 km^2.

Modeling lake size distributions using a power-law framework provides both a conceptual and quantitative tool to describe and compare glacial lake systems. These models enable statistical extrapolation beyond observed data, making them particularly valuable in glaciated basins where small lakes are numerous but often underrepresented due to resolution or mapping constraints. However, deviations below minimum area thresholds emphasize the need for careful parameterization when applying scaling models to lake inventories.

4. Conclusion

This study presents a high-resolution glacial lake inventory for the UIB using Sentinel-1 SAR imagery and an adaptive thresholding method. By focusing on a narrow seasonal window and leveraging the all-weather capabilities of SAR, the study addresses key limitations of previous optical-based inventories, particularly the under-detection of small and short-lived SGLs. The resulting dataset identifies 6,019 glacial lakes with a combined area of 266 km^2 in August 2023, providing the most up-to-date and comprehensive baseline for the region.

The spatial distribution of lakes in the UIB is strongly controlled by elevation and glacier dynamics. Most lakes occur between 4,000 and 4,600 m, coinciding with the primary glacierized area. Lake type distributions further illustrate the influence of glacial and geomorphic processes. GELs and MDLs dominate much of the basin, indicating advanced glacier retreat and overdeepened terrain, while SGLs are widespread in the Karakoram, which is characterized by stable debris-covered glaciers.

The variation in lake types and elevation patterns across the basin highlights the complex interplay of climate, glacier dynamics, and topography in shaping glacial lake systems across the UIB. The inventory provides a critical foundation for assessing glacial lake hazards, evaluating climate impacts, and monitoring future changes in one of the world's most glacierized basins.

Supplementary Materials: The following supporting information can be downloaded at the website of this paper posted on Preprints.org, Table S1: Summary of global and regional glacial lake inventories covering the UIB. The datasets were clipped to the UIB study area for comparison. The table lists the number of lakes and total lake area reported by each inventory within the study domain, along with the inventory years and the minimum lake area thresholds; Table S2: Summary of Willmott statistics evaluating the agreement between Sentinel-1-based glacial lake areas and manually delineated Sentinel-2 lake areas; Table S3: Power-law statistics for glacial lake size distributions across regions and lake types within the UIB.

Author Contributions: Conceptualization, I.K., J.M.J. (Jennifer M. Jacobs), J.M.J. (Jeremy M. Johnston), and M.V.; methodology, I.K.; software, I.K.; validation, I.K. and J.M.J. (Jennifer M. Jacobs); formal analysis, I.K.; investigation, I.K.; resources, J.M.J. (Jennifer M. Jacobs); data curation, I.K.; writing—original draft preparation, I.K.; writing—review and editing, I.K., J.M.J. (Jennifer M. Jacobs), J.M.J. (Jeremy M. Johnston), and M.V.; visualization, I.K., J.M.J (Jeremy M. Johnston), and M.V.; supervision, J.M.J. (Jennifer M. Jacobs); project administration, J.M.J. (Jennifer M. Jacobs); funding acquisition, I.K. All authors have read and agreed to the published version of the manuscript.

 doi:10.20944/preprints202509.0422.v1

Funding: This research was funded by a Fulbright Program grant sponsored by the Bureau of Educational and Cultural Affairs of the United States Department of State and administered by the Institute of International Education

Data Availability Statement: The original contributions presented in this study are included in the article/Supplementary Material. Further inquiries can be directed to the corresponding author.

Acknowledgments: The authors want to thank Joseph Licciardi and Cameron Wake for reviewing and providing feedback on the manuscript.

Conflicts of Interest: The authors declare no conflicts of interest. The funders had no role in the design of the study; in the collection, analyses, or interpretation of data; in the writing of the manuscript; or in the decision to publish the results.

Abbreviations

The following abbreviations are used in this manuscript:

α	Power-law Exponent
CCDF	Complementary Cumulative Distribution Functions
DEM	Digital Elevation Model
GEE	Google Earth Engine
GEL	Glacial Erosion Lake
GLOF	Glacial Lake Outburst Flood
GRD	Ground Range Detected
HMA	High Mountain Asia
IW	Interferometric Wide Swath
KS	Kolmogorov-Smirnov Statistic
MAE	Mean Absolute Error
MAPE	Mean Absolute Percent Error
MDL	Moraine-dammed Lake
NDSI	Normalized Difference Snow Index
NDWI	Normalized Difference Water Index
RGI	Randolph Glacier Inventory
RMSE	Root Mean Square Error
S1	Sentinel-1
S2	Sentinel-2
SAR	Synthetic Aperture Radar
SGL	Supraglacial Lake
SRTM	Shuttle Radar Topography Mission
UIB	Upper Indus Basin
VV	Vertical transmit – Vertical receive Polarization
x_{min}	Minimum Area Threshold (Power-law distribution)

References

1. Roe, G. H.; Baker, M. B.; Herla, F. Centennial Glacier Retreat as Categorical Evidence of Regional Climate Change. *Nat. Geosci.* **2017**, *10* (2), 95–99. https://doi.org/10.1038/ngeo2863.
2. Hugonnet, R.; McNabb, R.; Berthier, E.; Menounos, B.; Nuth, C.; Girod, L.; Farinotti, D.; Huss, M.; Dussaillant, I.; Brun, F.; Kääb, A. Accelerated Global Glacier Mass Loss in the Early Twenty-First Century. *Nature* **2021**, *592* (7856), 726–731. https://doi.org/10.1038/s41586-021-03436-z.
3. The GlaMBIE Team; Zemp, M.; Jakob, L.; Dussaillant, I.; Nussbaumer, S. U.; Gourmelen, N.; Dubber, S.; A, G.; Abdullahi, S.; Andreassen, L. M.; Berthier, E.; Bhattacharya, A.; Blazquez, A.; Boehm Vock, L. F.; Bolch, T.; Box, J.; Braun, M. H.; Brun, F.; Cicero, E.; Colgan, W.; Eckert, N.; Farinotti, D.; Florentine, C.; Floricioiu, D.; Gardner, A.; Harig, C.; Hassan, J.; Hugonnet, R.; Huss, M.; Jóhannesson, T.; Liang, C.-C. A.; Ke, C.-Q.; Khan, S. A.; King, O.; Kneib, M.; Krieger, L.; Maussion, F.; Mattea, E.; McNabb, R.; Menounos, B.; Miles, E.; Moholdt, G.; Nilsson, J.; Pálsson, F.; Pfeffer, J.; Piermattei, L.; Plummer, S.; Richter, A.; Sasgen, I.; Schuster,

 doi:10.20944/preprints202509.0422.v1

L.; Seehaus, T.; Shen, X.; Sommer, C.; Sutterley, T.; Treichler, D.; Velicogna, I.; Wouters, B.; Zekollari, H.; Zheng, W. Community Estimate of Global Glacier Mass Changes from 2000 to 2023. *Nature* **2025**, *639* (8054), 382–388. https://doi.org/10.1038/s41586-024-08545-z.

4. Wilson, R.; Glasser, N. F.; Reynolds, J. M.; Harrison, S.; Anacona, P. I.; Schaefer, M.; Shannon, S. Glacial Lakes of the Central and Patagonian Andes. *Glob. Planet. Change* **2018**, *162*, 275–291. https://doi.org/10.1016/j.gloplacha.2018.01.004.
5. Shugar, D. H.; Burr, A.; Haritashya, U. K.; Kargel, J. S.; Watson, C. S.; Kennedy, M. C.; Bevington, A. R.; Betts, R. A.; Harrison, S.; Strattman, K. Rapid Worldwide Growth of Glacial Lakes since 1990. *Nat. Clim. Change* **2020**, *10* (10), 939–945. https://doi.org/10.1038/s41558-020-0855-4.
6. Wang, X.; Guo, X.; Yang, C.; Liu, Q.; Wei, J.; Zhang, Y.; Liu, S.; Zhang, Y.; Jiang, Z.; Tang, Z. Glacial Lake Inventory of High-Mountain Asia in 1990 and 2018 Derived from Landsat Images. *Earth Syst. Sci. Data* **2020**, *12* (3), 2169–2182. https://doi.org/10.5194/essd-12-2169-2020.
7. Song, C.; Fan, C.; Ma, J.; Zhan, P.; Deng, X. A Spatially Constrained Remote Sensing-Based Inventory of Glacial Lakes Worldwide. *Sci. Data* **2025**, *12* (1), 464. https://doi.org/10.1038/s41597-025-04809-z.
8. Harrison, S.; Kargel, J. S.; Huggel, C.; Reynolds, J.; Shugar, D. H.; Betts, R. A.; Emmer, A.; Glasser, N.; Haritashya, U. K.; Klimeš, J.; Reinhardt, L.; Schaub, Y.; Wiltshire, A.; Regmi, D.; Vilímek, V. Climate Change and the Global Pattern of Moraine-Dammed Glacial Lake Outburst Floods. *The Cryosphere* **2018**, *12* (4), 1195–1209. https://doi.org/10.5194/tc-12-1195-2018.
9. Emmer, A.; Harrison, S.; Mergili, M.; Allen, S.; Frey, H.; Huggel, C. 70 Years of Lake Evolution and Glacial Lake Outburst Floods in the Cordillera Blanca (Peru) and Implications for the Future. *Geomorphology* **2020**, *365*, 107178. https://doi.org/10.1016/j.geomorph.2020.107178.
10. How, P.; Messerli, A.; Mätzler, E.; Santoro, M.; Wiesmann, A.; Caduff, R.; Langley, K.; Bojesen, M. H.; Paul, F.; Kääb, A.; Carrivick, J. L. Greenland-Wide Inventory of Ice Marginal Lakes Using a Multi-Method Approach. *Sci. Rep.* **2021**, *11* (1), 4481. https://doi.org/10.1038/s41598-021-83509-1.
11. Ma, J.; Song, C.; Wang, Y. Spatially and Temporally Resolved Monitoring of Glacial Lake Changes in Alps During the Recent Two Decades. *Front. Earth Sci.* **2021**, *9*, 723386. https://doi.org/10.3389/feart.2021.723386.
12. Mölg, N.; Huggel, C.; Herold, T.; Storck, F.; Allen, S.; Haeberli, W.; Schaub, Y.; Odermatt, D. Inventory and Evolution of Glacial Lakes since the Little Ice Age: Lessons from the Case of Switzerland. *Earth Surf. Process. Landf.* **2021**, *46* (13), 2551–2564. https://doi.org/10.1002/esp.5193.
13. Gupta, A.; Maheshwari, R.; Sweta; Guru, N.; Rao, B. S.; Raju, P. V.; Rao, V. V. Updated Glacial Lake Inventory of Indus River Basin Based on High-Resolution Indian Remote Sensing Satellite Data. *J. Indian Soc. Remote Sens.* **2022**, *50* (1), 73–98. https://doi.org/10.1007/s12524-021-01452-0.
14. Rick, B.; McGrath, D.; Armstrong, W.; McCoy, S. W. Dam Type and Lake Location Characterize Ice-Marginal Lake Area Change in Alaska and NW Canada between 1984 and 2019. *The Cryosphere* **2022**, *16* (1), 297–314. https://doi.org/10.5194/tc-16-297-2022.
15. Zhang, G.; Yao, T.; Xie, H.; Wang, W.; Yang, W. An Inventory of Glacial Lakes in the Third Pole Region and Their Changes in Response to Global Warming. *Glob. Planet. Change* **2015**, *131*, 148–157. https://doi.org/10.1016/j.gloplacha.2015.05.013.
16. Zhang, M.; Chen, F.; Tian, B. An Automated Method for Glacial Lake Mapping in High Mountain Asia Using Landsat 8 Imagery. *J. Mt. Sci.* **2018**, *15* (1), 13–24. https://doi.org/10.1007/s11629-017-4518-5.
17. Zhang, M.; Chen, F.; Zhao, H.; Wang, J.; Wang, N. Recent Changes of Glacial Lakes in the High Mountain Asia and Its Potential Controlling Factors Analysis. *Remote Sens.* **2021**, *13* (18), 3757. https://doi.org/10.3390/rs13183757.
18. Chen, F.; Zhang, M.; Guo, H.; Allen, S.; Kargel, J. S.; Haritashya, U. K.; Watson, C. S. Annual 30 m Dataset for Glacial Lakes in High Mountain Asia from 2008 to 2017. *Earth Syst. Sci. Data* **2021**, *13* (2), 741–766. https://doi.org/10.5194/essd-13-741-2021.
19. Zhang, B.; Liu, G.; Zhang, R.; Fu, Y.; Liu, Q.; Cai, J.; Wang, X.; Li, Z. Monitoring Dynamic Evolution of the Glacial Lakes by Using Time Series of Sentinel-1A SAR Images. *Remote Sens.* **2021**, *13* (7), 1313. https://doi.org/10.3390/rs13071313.

 doi:10.20944/preprints202509.0422.v1

20. Strozzi, T.; Wiesmann, A.; Kääb, A.; Joshi, S.; Mool, P. Glacial Lake Mapping with Very High Resolution Satellite SAR Data. *Nat. Hazards Earth Syst. Sci.* **2012**, *12* (8), 2487–2498. https://doi.org/10.5194/nhess-12-2487-2012.
21. Zhang, M.; Chen, F.; Tian, B.; Liang, D.; Yang, A. High-Frequency Glacial Lake Mapping Using Time Series of Sentinel-1A/1B SAR Imagery: An Assessment for the Southeastern Tibetan Plateau. *Int. J. Environ. Res. Public. Health* **2020**, *17* (3), 1072. https://doi.org/10.3390/ijerph17031072.
22. Dirscherl, M.; Dietz, A. J.; Kneisel, C.; Kuenzer, C. A Novel Method for Automated Supraglacial Lake Mapping in Antarctica Using Sentinel-1 SAR Imagery and Deep Learning. *Remote Sens.* **2021**, *13* (2), 197. https://doi.org/10.3390/rs13020197.
23. Wendleder, A.; Schmitt, A.; Erbertseder, T.; D'Angelo, P.; Mayer, C.; Braun, M. H. Seasonal Evolution of Supraglacial Lakes on Baltoro Glacier From 2016 to 2020. *Front. Earth Sci.* **2021**, *9*, 725394. https://doi.org/10.3389/feart.2021.725394.
24. Luo, X.; Hu, Z.; Liu, L. Investigating the Seasonal Dynamics of Surface Water over the Qinghai–Tibet Plateau Using Sentinel-1 Imagery and a Novel Gated Multiscale ConvNet. *Int. J. Digit. Earth* **2023**, *16* (1), 1372–1394. https://doi.org/10.1080/17538947.2023.2198266.
25. Miles, K. E.; Willis, I. C.; Benedek, C. L.; Williamson, A. G.; Tedesco, M. Toward Monitoring Surface and Subsurface Lakes on the Greenland Ice Sheet Using Sentinel-1 SAR and Landsat-8 OLI Imagery. *Front. Earth Sci.* **2017**, *5*, 58. https://doi.org/10.3389/feart.2017.00058.
26. Wangchuk, S.; Bolch, T. Mapping of Glacial Lakes Using Sentinel-1 and Sentinel-2 Data and a Random Forest Classifier: Strengths and Challenges. *Sci. Remote Sens.* **2020**, *2*. https://doi.org/10.1016/j.srs.2020.100008.
27. Wu, R.; Liu, G.; Zhang, R.; Wang, X.; Li, Y.; Zhang, B.; Cai, J.; Xiang, W. A Deep Learning Method for Mapping Glacial Lakes from the Combined Use of Synthetic-Aperture Radar and Optical Satellite Images. *Remote Sens.* **2020**, *12* (24), 4020. https://doi.org/10.3390/rs12244020.
28. Wang, W.; Xiang, Y.; Gao, Y.; Lu, A.; Yao, T. Rapid Expansion of Glacial Lakes Caused by Climate and Glacier Retreat in the Central Himalayas: RAPID EXPANSION OF GLACIAL LAKES IN THE CENTRAL HIMALAYAS. *Hydrol. Process.* **2015**, *29* (6), 859–874. https://doi.org/10.1002/hyp.10199.
29. Watson, C. S.; King, O.; Miles, E. S.; Quincey, D. J. Optimising NDWI Supraglacial Pond Classification on Himalayan Debris-Covered Glaciers. *Remote Sens. Environ.* **2018**, *217*, 414–425. https://doi.org/10.1016/j.rse.2018.08.020.
30. Racoviteanu, A.; Williams, M.; Barry, R. Optical Remote Sensing of Glacier Characteristics: A Review with Focus on the Himalaya. *Sensors* **2008**, *8* (5), 3355–3383. https://doi.org/10.3390/s8053355.
31. Jawak, S. D.; Bidawe, T. G.; Luis, A. J. A Review on Applications of Imaging Synthetic Aperture Radar with a Special Focus on Cryospheric Studies. *Adv. Remote Sens.* **2015**, *04* (02), 163–175. https://doi.org/10.4236/ars.2015.42014.
32. Lutz, A. F.; Immerzeel, W. W.; Kraaijenbrink, P. D.; Shrestha, A. B.; Bierkens, M. F. Climate Change Impacts on the Upper Indus Hydrology: Sources, Shifts and Extremes. *PLoS One* **2016**, *11* (11), e0165630. https://doi.org/10.1371/journal.pone.0165630.
33. Bajracharya, S. R.; Shrestha, B. *The Status of Glaciers in the Hindu Kush-Himalayan Region*, 0 ed.; International Centre for Integrated Mountain Development (ICIMOD): Kathmandu, Nepal, 2011. https://doi.org/10.53055/ICIMOD.551.
34. RGI Consortium. Randolph Glacier Inventory - A Dataset of Global Glacier Outlines, Version 6, 2017. https://doi.org/10.7265/4M1F-GD79.
35. Giese, A.; Rupper, S.; Keeler, D.; Johnson, E.; Forster, R. Indus River Basin Glacier Melt at the Subbasin Scale. *Front. Earth Sci.* **2022**, *10*, 767411. https://doi.org/10.3389/feart.2022.767411.
36. Lutz, A. F.; Immerzeel, W. W.; Shrestha, A. B.; Bierkens, M. F. P. Consistent Increase in High Asia's Runoff Due to Increasing Glacier Melt and Precipitation. *Nat. Clim. Change* **2014**, *4* (7), 587–592. https://doi.org/10.1038/nclimate2237.
37. Azam, Mohd. F.; Kargel, J. S.; Shea, J. M.; Nepal, S.; Haritashya, U. K.; Srivastava, S.; Maussion, F.; Qazi, N.; Chevallier, P.; Dimri, A. P.; Kulkarni, A. V.; Cogley, J. G.; Bahuguna, I. Glaciohydrology of the Himalaya-Karakoram. *Science* **2021**, *373* (6557), eabf3668. https://doi.org/10.1126/science.abf3668.

 doi:10.20944/preprints202509.0422.v1

38. Orr, A.; Ahmad, B.; Alam, U.; Appadurai, A.; Bharucha, Z. P.; Biemans, H.; Bolch, T.; Chaulagain, N. P.; Dhaubanjar, S.; Dimri, A. P.; Dixon, H.; Fowler, H. J.; Gioli, G.; Halvorson, S. J.; Hussain, A.; Jeelani, G.; Kamal, S.; Khalid, I. S.; Liu, S.; Lutz, A.; Mehra, M. K.; Miles, E.; Momblanch, A.; Muccione, V.; Mukherji, A.; Mustafa, D.; Najmuddin, O.; Nasimi, M. N.; Nüsser, M.; Pandey, V. P.; Parveen, S.; Pellicciotti, F.; Pollino, C.; Potter, E.; Qazizada, M. R.; Ray, S.; Romshoo, S.; Sarkar, S. K.; Sawas, A.; Sen, S.; Shah, A.; Shah, M. A. A.; Shea, J. M.; Sheikh, A. T.; Shrestha, A. B.; Tayal, S.; Tigala, S.; Virk, Z. T.; Wester, P.; Wescoat, J. L. Knowledge Priorities on Climate Change and Water in the Upper Indus Basin: A Horizon Scanning Exercise to Identify the Top 100 Research Questions in Social and Natural Sciences. *Earths Future* **2022**, *10* (4). https://doi.org/10.1029/2021ef002619.
39. Immerzeel, W. W.; Bierkens, M. F. P. Asia's Water Balance. *Nat. Geosci.* **2012**, *5* (12), 841–842. https://doi.org/10.1038/ngeo1643.
40. Lund, J.; Forster, R. R.; Rupper, S. B.; Deeb, E. J.; Marshall, H. P.; Hashmi, M. Z.; Burgess, E. Mapping Snowmelt Progression in the Upper Indus Basin With Synthetic Aperture Radar. *Front. Earth Sci.* **2020**, *7*. https://doi.org/10.3389/feart.2019.00318.
41. Hasan, H.; Hashmi, M. Z. U. R.; Ahmed, S. I.; Anees, M. Assessing Climate Sensitivity of the Upper Indus Basin Using Fully Distributed, Physically-Based Hydrologic Modeling and Multi-Model Climate Ensemble Approach. *Sci. Rep.* **2025**, *15* (1), 4109. https://doi.org/10.1038/s41598-024-84975-z.
42. Jabbar, A.; Othman, A. A.; Merkel, B.; Hasan, S. E. Change Detection of Glaciers and Snow Cover and Temperature Using Remote Sensing and GIS: A Case Study of the Upper Indus Basin, Pakistan. *Remote Sens. Appl. Soc. Environ.* **2020**, *18*. https://doi.org/10.1016/j.rsase.2020.100308.
43. Wake, C. P. Glaciochemical Investigations as a Tool for Determining the Spatial and Seasonal Variation of Snow Accumulation in the Central Karakoram, Northern Pakistan. *Ann. Glaciol.* **1989**, *13*, 279–284. https://doi.org/10.3189/s0260305500008053.
44. Maussion, F.; Scherer, D.; Mölg, T.; Collier, E.; Curio, J.; Finkelnburg, R. Precipitation Seasonality and Variability over the Tibetan Plateau as Resolved by the High Asia Reanalysis*. *J. Clim.* **2014**, *27* (5), 1910–1927. https://doi.org/10.1175/jcli-d-13-00282.1.
45. Hussain, A.; Cao, J.; Hussain, I.; Begum, S.; Akhtar, M.; Wu, X.; Guan, Y.; Zhou, J. Observed Trends and Variability of Temperature and Precipitation and Their Global Teleconnections in the Upper Indus Basin, Hindukush-Karakoram-Himalaya. *Atmosphere* **2021**, *12* (8), 973. https://doi.org/10.3390/atmos12080973.
46. Khan, A.; Koch, M. Correction and Informed Regionalization of Precipitation Data in a High Mountainous Region (Upper Indus Basin) and Its Effect on SWAT-Modelled Discharge. *Water* **2018**, *10* (11), 1557. https://doi.org/10.3390/w10111557.
47. Demissie, B.; Vanhuysse, S.; Grippa, T.; Flasse, C.; Wolff, E. Using Sentinel-1 and Google Earth Engine Cloud Computing for Detecting Historical Flood Hazards in Tropical Urban Regions: A Case of Dar Es Salaam. *Geomat. Nat. Hazards Risk* **2023**, *14* (1), 2202296. https://doi.org/10.1080/19475705.2023.2202296.
48. Shamsaie, R.; Ghaderi, D. Comparison of Efficiency of Spectral (NDWI) and SAR (GRD) Method in Shoreline Detection: A Novel Method of Integrating GRD and SLC Products of Sentinel-1 Satellite. *Reg. Stud. Mar. Sci.* **2025**, *84*, 104132. https://doi.org/10.1016/j.rsma.2025.104132.
49. Jiang, D.; Li, S.; Hajnsek, I.; Siddique, M. A.; Hong, W.; Wu, Y. Glacial Lake Mapping Using Remote Sensing Geo-Foundation Model. *Int. J. Appl. Earth Obs. Geoinformation* **2025**, *136*, 104371. https://doi.org/10.1016/j.jag.2025.104371.
50. Farr, T. G.; Rosen, P. A.; Caro, E.; Crippen, R.; Duren, R.; Hensley, S.; Kobrick, M.; Paller, M.; Rodriguez, E.; Roth, L.; Seal, D.; Shaffer, S.; Shimada, J.; Umland, J.; Werner, M.; Oskin, M.; Burbank, D.; Alsdorf, D. The Shuttle Radar Topography Mission. *Rev. Geophys.* **2007**, *45* (2), 2005RG000183. https://doi.org/10.1029/2005RG000183.
51. Vollrath, A.; Mullissa, A.; Reiche, J. Angular-Based Radiometric Slope Correction for Sentinel-1 on Google Earth Engine. *Remote Sens.* **2020**, *12* (11), 1867. https://doi.org/10.3390/rs12111867.
52. Mullissa, A.; Vollrath, A.; Odongo-Braun, C.; Slagter, B.; Balling, J.; Gou, Y.; Gorelick, N.; Reiche, J. Sentinel-1 SAR Backscatter Analysis Ready Data Preparation in Google Earth Engine. *Remote Sens.* **2021**, *13* (10), 1954. https://doi.org/10.3390/rs13101954.

 doi:10.20944/preprints202509.0422.v1

53. Small, D. Flattening Gamma: Radiometric Terrain Correction for SAR Imagery. *IEEE Trans. Geosci. Remote Sens.* **2011**, *49* (8), 3081–3093. https://doi.org/10.1109/TGRS.2011.2120616.
54. Zhang, Y.; Zhao, J.; Yao, X.; Duan, H.; Yang, J.; Pang, W. Inventory of Glacial Lake in the Southeastern Qinghai-Tibet Plateau Derived from Sentinel-1 SAR Image and Sentinel-2 MSI Image. *Remote Sens.* **2023**, *15* (21), 5142. https://doi.org/10.3390/rs15215142.
55. Otsu, N. A Threshold Selection Method from Gray-Level Histograms. *IEEE Trans. Syst. Man Cybern.* **1979**, *9* (1), 62–66. https://doi.org/10.1109/TSMC.1979.4310076.
56. Alstott, J.; Bullmore, E.; Plenz, D. Powerlaw: A Python Package for Analysis of Heavy-Tailed Distributions. *PLoS ONE* **2014**, *9* (1), e85777. https://doi.org/10.1371/journal.pone.0085777.
57. Wangchuk, S.; Bolch, T.; Robson, B. A. Monitoring Glacial Lake Outburst Flood Susceptibility Using Sentinel-1 SAR Data, Google Earth Engine, and Persistent Scatterer Interferometry. *Remote Sens. Environ.* **2022**, *271*. https://doi.org/10.1016/j.rse.2022.112910.
58. Wei, Y.; Jia, L.; Ma, X.; Lei, Z. Development Genetic and Stability Classification of Seasonal Glacial Lakes in a Tectonically Active Area—A Case Study in Niangmuco, East Margin of the Eastern Himalayan Syntaxis. *Front. Earth Sci.* **2024**, *12*, 1361889. https://doi.org/10.3389/feart.2024.1361889.
59. Hewitt, K. Glacier Change, Concentration, and Elevation Effects in the Karakoram Himalaya, Upper Indus Basin. *Mt. Res. Dev.* **2011**, *31* (3), 188–200. https://doi.org/10.1659/mrd-journal-d-11-00020.1.
60. Romshoo, S. A.; Abdullah, T.; Ameen, U.; Bhat, M. H. Glacier Thickness and Volume Estimation in the Upper Indus Basin Using Modeling and Ground Penetrating Radar Measurements. *Ann. Glaciol.* **2023**, *64* (92), 385–395. https://doi.org/10.1017/aog.2024.2.
61. Song, C.; Sheng, Y. Contrasting Evolution Patterns between Glacier-Fed and Non-Glacier-Fed Lakes in the Tanggula Mountains and Climate Cause Analysis. *Clim. Change* **2016**, *135* (3–4), 493–507. https://doi.org/10.1007/s10584-015-1578-9.
62. Yang, Z.; Duan, S.-B.; Dai, X.; Sun, Y.; Liu, M. Mapping of Lakes in the Qinghai-Tibet Plateau from 2016 to 2021: Trend and Potential Regularity. *Int. J. Digit. Earth* **2022**, *15* (1), 1692–1714. https://doi.org/10.1080/17538947.2022.2131008.
63. Li, Y.; Liao, J.; Guo, H.; Liu, Z.; Shen, G. Patterns and Potential Drivers of Dramatic Changes in Tibetan Lakes, 1972–2010. *PLoS ONE* **2014**, *9* (11), e111890. https://doi.org/10.1371/journal.pone.0111890.
64. Zhang, G.; Yao, T.; Piao, S.; Bolch, T.; Xie, H.; Chen, D.; Gao, Y.; O'Reilly, C. M.; Shum, C. K.; Yang, K.; Yi, S.; Lei, Y.; Wang, W.; He, Y.; Shang, K.; Yang, X.; Zhang, H. Extensive and Drastically Different Alpine Lake Changes on Asia's High Plateaus during the Past Four Decades. *Geophys. Res. Lett.* **2017**, *44* (1), 252–260. https://doi.org/10.1002/2016GL072033.
65. Prakash, C.; Nagarajan, R. Glacial Lake Inventory and Evolution in Northwestern Indian Himalaya. *IEEE J. Sel. Top. Appl. Earth Obs. Remote Sens.* **2017**, *10* (12), 5284–5294. https://doi.org/10.1109/JSTARS.2017.2767098.
66. Banerjee, P.; Bhuiyan, C. Glacial Lakes of Sikkim Himalaya: Their Dynamics, Trends, and Likely Fate—a Timeseries Analysis through Cloud-Based Geocomputing, and Machine Learning. *Geomat. Nat. Hazards Risk* **2023**, *14* (1), 2286903. https://doi.org/10.1080/19475705.2023.2286903.
67. Mohanty, L.; Maiti, S.; Dixit, A. Spatio-Temporal Assessment of Regional Scale Evolution and Distribution of Glacial Lakes in Himalaya. *Front. Earth Sci.* **2023**, *10*, 1038777. https://doi.org/10.3389/feart.2022.1038777.
68. Das, S.; Das, S.; Mandal, S. T.; Sharma, M. C.; Ramsankaran, R. Inventory and GLOF Susceptibility of Glacial Lakes in Chenab Basin, Western Himalaya. *Geomat. Nat. Hazards Risk* **2024**, *15* (1), 2356216. https://doi.org/10.1080/19475705.2024.2356216.
69. Dou, X.; Fan, X.; Wang, X.; Yunus, A. P.; Xiong, J.; Tang, R.; Lovati, M.; van Westen, C.; Xu, Q. Spatio-Temporal Evolution of Glacial Lakes in the Tibetan Plateau over the Past 30 Years. *Remote Sens.* **2023**, *15* (2), 416. https://doi.org/10.3390/rs15020416.
70. Buckel, J.; Otto, J. C.; Prasicek, G.; Keuschnig, M. Glacial Lakes in Austria - Distribution and Formation since the Little Ice Age. *Glob. Planet. Change* **2018**, *164*, 39–51. https://doi.org/10.1016/j.gloplacha.2018.03.003.
71. Wood, J. L.; Harrison, S.; Wilson, R.; Emmer, A.; Yarleque, C.; Glasser, N. F.; Torres, J. C.; Caballero, A.; Araujo, J.; Bennett, G. L.; Diaz-Moreno, A.; Garay, D.; Jara, H.; Poma, C.; Reynolds, J. M.; Riveros, C. A.;

 doi:10.20944/preprints202509.0422.v1

Romero, E.; Shannon, S.; Tinoco, T.; Turpo, E.; Villafane, H. Contemporary Glacial Lakes in the Peruvian Andes. *Glob. Planet. Change* **2021**, *204*, 103574. https://doi.org/10.1016/j.gloplacha.2021.103574.

72. Kroczek, T.; Vilímek, V. Glacial Lakes Inventory and Susceptibility Assessment in the Alsek River Basin, Yukon, Canada. *Geoenvironmental Disasters* **2024**, *11* (1), 42. https://doi.org/10.1186/s40677-024-00304-6.
73. Colonia, D.; Torres, J.; Haeberli, W.; Schauwecker, S.; Braendle, E.; Giraldez, C.; Cochachin, A. Compiling an Inventory of Glacier-Bed Overdeepenings and Potential New Lakes in De-Glaciating Areas of the Peruvian Andes: Approach, First Results, and Perspectives for Adaptation to Climate Change. *Water* **2017**, *9* (5), 336. https://doi.org/10.3390/w9050336.
74. King, O.; Dehecq, A.; Quincey, D.; Carrivick, J. Contrasting Geometric and Dynamic Evolution of Lake and Land-Terminating Glaciers in the Central Himalaya. *Glob. Planet. Change* **2018**, *167*, 46–60. https://doi.org/10.1016/j.gloplacha.2018.05.006.
75. Raj, K. B. G.; Kumar, K. V. Inventory of Glacial Lakes and Its Evolution in Uttarakhand Himalaya Using Time Series Satellite Data. *J. Indian Soc. Remote Sens.* **2016**, *44* (6), 959–976. https://doi.org/10.1007/s12524-016-0560-y.
76. Lee, E.; Carrivick, J. L.; Quincey, D. J.; Cook, S. J.; James, W. H. M.; Brown, L. E. Accelerated Mass Loss of Himalayan Glaciers since the Little Ice Age. *Sci. Rep.* **2021**, *11* (1), 24284. https://doi.org/10.1038/s41598-021-03805-8.
77. Farinotti, D.; Immerzeel, W. W.; De Kok, R. J.; Quincey, D. J.; Dehecq, A. Manifestations and Mechanisms of the Karakoram Glacier Anomaly. *Nat. Geosci.* **2020**, *13* (1), 8–16. https://doi.org/10.1038/s41561-019-0513-5.
78. Qureshi, M. A.; Li, Y.; Yi, C.; Xu, X. Glacial Changes in the Hunza Basin, Western Karakoram, since the Little Ice Age. *Palaeogeogr. Palaeoclimatol. Palaeoecol.* **2021**, *562*, 110086. https://doi.org/10.1016/j.palaeo.2020.110086.
79. Nie, Y.; Sheng, Y.; Liu, Q.; Liu, L.; Liu, S.; Zhang, Y.; Song, C. A Regional-Scale Assessment of Himalayan Glacial Lake Changes Using Satellite Observations from 1990 to 2015. *Remote Sens. Environ.* **2017**, *189*, 1–13. https://doi.org/10.1016/j.rse.2016.11.008.
80. Wendleder, A.; Friedl, P.; Mayer, C. Impacts of Climate and Supraglacial Lakes on the Surface Velocity of Baltoro Glacier from 1992 to 2017. *Remote Sens.* **2018**, *10* (11), 1681. https://doi.org/10.3390/rs10111681.
81. Yao, X.; Liu, S.; Han, L.; Sun, M.; Zhao, L. Definition and Classification System of Glacial Lake for Inventory and Hazards Study. *J. Geogr. Sci.* **2018**, *28* (2), 193–205. https://doi.org/10.1007/s11442-018-1467-z.
82. Richardson, S. D.; Reynolds, J. M. An Overview of Glacial Hazards in the Himalayas. *Quat. Int.* **2000**, *65–66*, 31–47. https://doi.org/10.1016/S1040-6182(99)00035-X.
83. Thakuri, S.; Salerno, F.; Bolch, T.; Guyennon, N.; Tartari, G. Factors Controlling the Accelerated Expansion of Imja Lake, Mount Everest Region, Nepal. *Ann. Glaciol.* **2016**, *57* (71), 245–257. https://doi.org/10.3189/2016AoG71A063.
84. Haritashya, U. K.; Kargel, J. S.; Shugar, D. H.; Leonard, G. J.; Strattman, K.; Watson, C. S.; Shean, D.; Harrison, S.; Mandli, K. T.; Regmi, D. Evolution and Controls of Large Glacial Lakes in the Nepal Himalaya. *Remote Sens.* **2018**, *10* (5), 798. https://doi.org/10.3390/rs10050798.
85. King, O.; Bhattacharya, A.; Bhambri, R.; Bolch, T. Glacial Lakes Exacerbate Himalayan Glacier Mass Loss. *Sci Rep* **2019**, *9* (1), 18145. https://doi.org/10.1038/s41598-019-53733-x.
86. Maurer, J. M.; Schaefer, J. M.; Rupper, S.; Corley, A. Acceleration of Ice Loss across the Himalayas over the Past 40 Years. *Sci. Adv.* **2019**, *5* (6), eaav7266. https://doi.org/10.1126/sciadv.aav7266.
87. Pronk, J. B.; Bolch, T.; King, O.; Wouters, B.; Benn, D. I. Contrasting Surface Velocities between Lake- and Land-Terminating Glaciers in the Himalayan Region. *The Cryosphere* **2021**, *15* (12), 5577–5599. https://doi.org/10.5194/tc-15-5577-2021.
88. Cael, B. B.; Seekell, D. A. The Size-Distribution of Earth's Lakes. *Sci. Rep.* **2016**, *6* (1), 29633. https://doi.org/10.1038/srep29633.
89. Levenson, E. S.; Cooley, S.; Mullen, A.; Webb, E. E.; Watts, J. Glacial History Modifies Permafrost Controls on the Distribution of Lakes and Ponds. *Geophys. Res. Lett.* **2025**, *52* (4), e2024GL112771. https://doi.org/10.1029/2024GL112771.

 doi:10.20944/preprints202509.0422.v1

90. Zhang, T.; Wang, W.; An, B. A Conceptual Model for Glacial Lake Bathymetric Distribution. *The Cryosphere* **2023**, *17* (12), 5137–5154. https://doi.org/10.5194/tc-17-5137-2023.
91. Zhang, T.; Wang, W.; An, B. Heterogeneous Changes in Global Glacial Lakes under Coupled Climate Warming and Glacier Thinning. *Commun. Earth Environ.* **2024**, *5* (1), 374. https://doi.org/10.1038/s43247-024-01544-y.
92. Xu, F.; Coco, G.; Zhou, Z.; Townend, I.; Guo, L.; He, Q. A Universal Form of Power Law Relationships for River and Stream Channels. *Geophys. Res. Lett.* **2020**, *47* (20), e2020GL090493. https://doi.org/10.1029/2020GL090493.
93. Jones, K. E.; Howarth, J. D.; Massey, C. I.; Luković, B.; Sirguey, P.; Singeisen, C.; Gasston, C.; Morgenstern, R.; Ries, W. An Alternative to Landslide Volume-Area Scaling Relationships: An Ensemble Approach Adopting a Difference Model to Estimate the Total Volume of Landsliding Triggered by the 2016 Kaikōura Earthquake, New Zealand. *Landslides* **2025**. https://doi.org/10.1007/s10346-025-02479-x.